Automatic Shielding-Shimming Magnetic Field Compensator for Excluded Volume Applications

Guillermo O. Forte, Germán Farrher, Luis R. Canali, *Senior Member, IEEE*, and Esteban Anoardo

***Abstract*—We discuss the problem of automatic magnetic field compensation within an excluded volume where the magnetic field cannot be sensed in a direct way. Both magnetic field spatial average (shielding) and first order orthogonal gradients (shimming) are considered. The active shielding-shimming compensator is based on a multiple-input multiple-output controller driving a specifically designed coil-set. The magnetic field and its gradients are calculated from the readings of ten hall sensors located outside the exclusion volume.**

***Index Terms*—Active shielding, active shimming, excluded volume, fast field cycling nuclear magnetic resonance (FFC-NMR), magnetic field compensation, multiple-input multiple-output (MIMO) control.**

I. Introduction

SELECTED applications may require the cancellation of external time dependent magnetic fields within an exclusion volume. A specific example can be found in fast-field-cycling nuclear magnetic resonance (FFC-NMR), where for certain experimental protocols, external magnetic field contributions must be compensated at the ultra low frequency (ULF) limit. The experimental situation has already been described in an earlier publication [1].

In this paper we refer as "active magnetic field compensation" to the more general idea of simultaneous cancellation of the time dependent spatial average magnetic field and magnetic field gradient across an excluded volume. The problem of a combined shielding-shimming (SHISHI) active compensation becomes more complex the higher the order required for the shimming.

There appear to be no previous results concerning this approach. The use of active shielding in combination with shimming is used in magnetic resonance imaging to decouple the shimming fields from the main magnetic field. However, the purpose of this work is to compensate magnetic field inhomogeneities while actively canceling time-dependent external contributions within an exclusion volume of interest.

Manuscript received December 19, 2008; revised June 16, 2009; accepted August 01, 2009. Manuscript received in final form August 06, 2009. First published October 09, 2009; current version published June 23, 2010. This work was supported in part by Foncyt, in part by CONICET, and in part by Secyt-UNC. Recommended by Associate Editor N. K. Kazantzis.

G. O. Forte, G. Farrher, and E. Anoardo are with the LaRTE, Grupo de Resonancia Magnética Nuclear, Facultad de Matemática Astronomía y Física, Universidad Nacional de Córdoba e Instituto de Física Enrique Gaviola (CONICET), Argentina (e-mail: anoardo@famaf.unc.edu.ar; forte@famaf.unc.edu.ar).

L. R. Canali is with the CIII—Universidad Tecnológica Nacional, Facultad Regional Córdoba, Argentina.

Digital Object Identifier 10.1109/TCST.2009.2030174

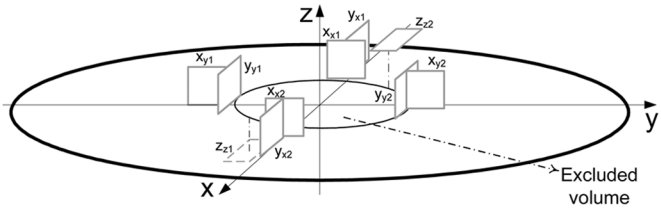

Fig. 1. Hall sensors probe. Each sensor measures the magnetic field perpendicular to the package face.

We will simplify the problem by considering first order gradients along the Cartesian orthogonal components only. The approach, as considered, has the basic weakness that such an elemental shimming can only be considered for specific low-resolution NMR applications.

Different strategies have been used to deal with the problem of active shielding control. Both analog [5] and digital [7] controllers are feasible. In the present work, a two-step compensator approach was used to solve the multivariable control problem. First, a decoupler counteracts the interactions between the controlled variables resulting in a more diagonal and easier to control plant. Then, the weakly interacting plant was controlled using standard methods like those used in single-input single-output (SISO) systems. Simple proportional, integrative and derivative (PID) circuits were used for each loop of the multivariable diagonal controller.

Just to test the concept, the device under study operates at a maximum frequency of about 150 Hz. The controlled variables are the mean magnetic field components and the first order magnetic field gradients along the Cartesian axes across the sample. Their respective values are obtained by combining the measurements of 10 Hall sensors contained in a special probe (see Fig. 1)

$$\left.\begin{array}{c} B_x = \frac{X_{x1}+X_{x2}+X_{y1}+X_{y2}}{4}, \\ B_y = \frac{Y_{x1}+Y_{x2}+Y_{y1}+Y_{y2}}{4}, B_z = \frac{Z_{z1}+Z_{z2}}{2}. \end{array}\right\} \quad (1)$$

$$\left.\begin{array}{c} G_{xx} = \frac{\partial B_x}{\partial x} = X_{x2} - X_{x1} \\ G_{\mathrm{yy}} = \frac{\partial B_y}{\partial y} = Y_{y2} - Y_{y1}, G_{zz} = \frac{\partial B_z}{\partial z} = 2(Z_{z2} - Z_{z1}). \end{array}\right\} \quad (2)$$

$B_i (i = x, y, z)$ are the mean magnetic field values calculated at the center of the excluded volume, G_{ii} the mentioned gradients and $X_{x1}, X_{x2}, X_{y1}, X_{y2}, Y_{x1}, Y_{x2}, Y_{y1}, Y_{y2}, Z_{z1}, Z_{z2}$ are the readings of the sensors.

As the references for the magnetic field components and gradients are set to zero, the inputs for the control algorithm are directly the calculated feedback signals. The algorithm provides the control signals u for each actuator. Each manipulated variable will drive the current of the corresponding compensating coil, thus generating the desired compensating magnetic field.

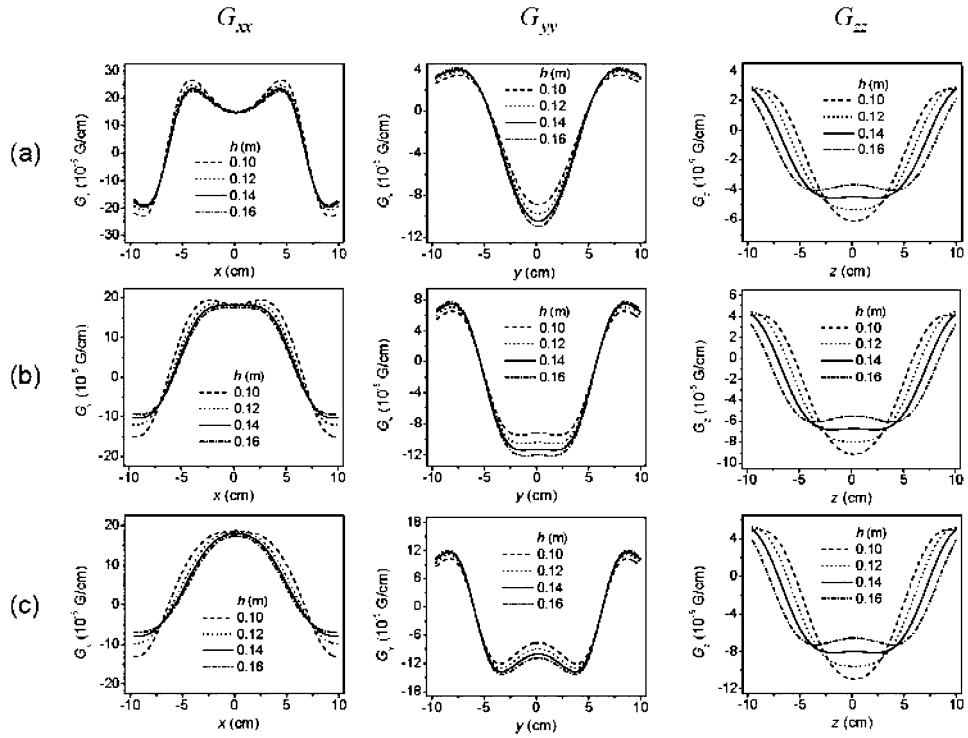

Fig. 2. Magnetic field gradient as a function of the position for (a) $\theta = \pi/3$, (b) $\theta = \pi/2$, (c) $\theta = 3\pi/5$ and different values of h. Each column corresponds to the gradient along a Cartesian direction.

For the sake of simplicity, the control system itself was developed within PC environment.

II. Simplified Shishi Coil-Set

A system composed by three coils was used to cancel the components B_x, B_y and B_z. A pair of Saddle-type coils were used for B_x and B_y while a Helmholtz-type for B_z. The coil-set was optimized to generate a homogeneous field within the excluded volume. The optimal geometry for the Saddle configuration was discussed in a previous work [2]. For a coil with radius R, height h and aperture angle θ, the optimal homogeneous magnetic field is obtained for $\theta = 2\pi/3$ and $h = 4R$. For a Helmholtz coil, the optimal configuration is when $h = R, h$ being in this case the gap between the two coils along the symmetry axis of the array.

The magnetic field gradient is a tensor defined by nine components: $\mathrm{G_{xx}}, \mathrm{G_{xy}}, \mathrm{G_{xz}}, \mathrm{G_{yx}}, \mathrm{G_{yy}}, \mathrm{G_{yz}}, \mathrm{G_{zx}}, \mathrm{G_{zy}}, \mathrm{G_{zz}}$. For the sake of simplicity we will focus only in the main components G_{xx}, G_{yy} and G_{zz}. Moreover, we assume that the external gradient is uniform within the excluded volume. These components are related through the Gauss's law for magnetism. That is, one is determined by the two others.

Therefore, a system consisting of only two coils is enough to cancel the external magnetic field gradients. As a consequence, an antiSaddle configuration was selected. For the design of the optimal coil-set we have to calculate the optimal values of the geometrical parameters R, h and θ that maximize the gradient along the desired direction, while simultaneously considering the spatial uniformity within the excluded volume. As a first step, the Biot-Savart's law and numerical simulations were used to calculate the magnetic field in the space (using C++).

As external gradients are supposed to be constant around the geometrical center of the excluded volume, the corresponding compensating coils should also present a low spatial-dependence around this point. The configuration was analyzed by varying the three parameters R, h and θ independently. The magnetic field gradients $G_{xx}(x), G_{yy}(y)$ and $G_{zz}(z)$ were determined for three different aperture angles ($\theta = \pi/3, \theta = \pi/2$ and $\theta = 3\pi/5$), and several values of h (see Fig. 2(a), (b) and (c)). The gradients were calculated for an electric current of 1 A through a single-loop-coil. It can be observed in the figure that for $\theta = \pi/2$ and h between 13 cm and 14 cm, the magnetic field gradient is almost constant along x, y and z simultaneously in a region of about 5 cm.

Fig. 3 shows the magnetic field gradient on the (x, y) plane at $z = 0$ position for the three different angles and $h = 13.5$ cm. It can be seen that the best configuration corresponds to the case of Fig. 3(b). The complete coil-set is shown in Fig. 4.

III. Control Algorithm

A two-step procedure was applied to design the controller [11].

1) Design of a "pre-compensator" to deal with the interactions in the plant.
2) Development of a diagonal controller based on a multi-SISO approach.

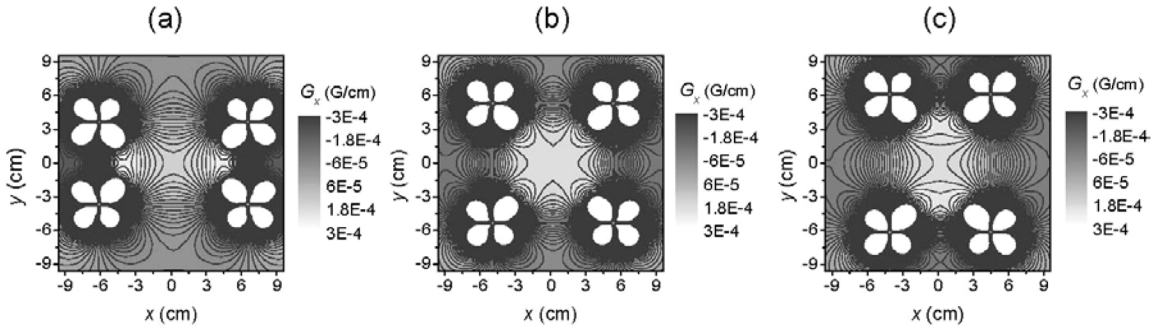

Fig. 3. Magnetic field gradient maps calculated for the (x, y) plane at $z = 0$ for (a) $\theta = \pi/3$, (b) $\theta = \pi/2$ and (c) $\theta = 3\pi/5$, and $h = 13.5$ cm. Case (b) corresponds to the optimal configuration where the gradient is uniform within a larger spatial region within the plane.

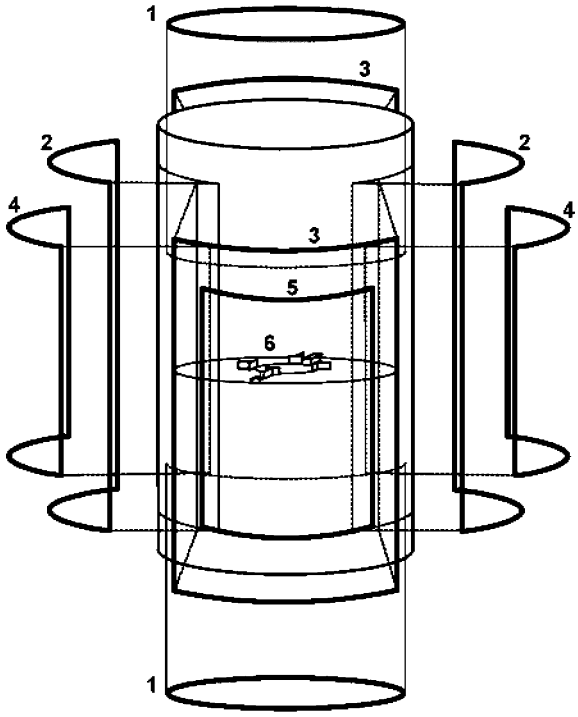

Fig. 4. Experimental setup diagram. 1—Helmholtz pair used to cancel B_z. 2—Saddle pair used to compensate B_x. 3—Saddle pair to compensate B_y. 4—Anti-Saddle pair used to shim G_{xx}. 5—Anti-Saddle pair for G_{yy}. 6—Hall probe (see details in Fig. 1).

In this section we rename the controlled variables as follows:

$$c_1 = \frac{\partial B_x}{\partial x}, \quad c_2 = \frac{\partial B_y}{\partial y}, \quad c_3 = B_x, \\ c_4 = B_y \quad c_5 = B_z. \tag{3}$$

A. Model of the Plant

As a first step we studied the steady-state effect of each control signal onto the different controlled variables signals. After a tedious math or complex simulations it would be possible to analytically determine the magnetic field produced by the coil-set at any point in the space. However, the experimental evaluation of the plant has the attractiveness of being much more realistic (mainly due to mechanical imperfections that are difficult to quantify). The resulting information is contained within the relative gain array (RGA) matrix [3], obtained from the steady-state gain matrix (SSGM)

$$\text{SSGM} = \begin{bmatrix} K_{11} & \cdot & K_{1n} \\ \cdot & \cdot & \cdot \\ K_{n1} & \cdot & K_{nn} \end{bmatrix}, \quad K_{\text{ij}} = \left.\frac{c_i}{u_j}\right|_u \\ \forall i = 1, \ldots\ldots\ldots, n; j = 1, \ldots\ldots\ldots, n. \tag{4}$$

Here

- n are the number of inputs and outputs of the plant (in our case $n = 5$);
- u_1 and u_2 are the command signals for the current sources driving the G_{xx} and G_{yy} coils respectively (with corresponding feedback signals c_1 and c_2);
- u_3 to u_5 are the command signals for the current sources driving the x, y and z homogeneous magnetic field coils respectively (feedback signals are c_3 to c_5);
- u_j is an integer number proportional to the current flowing through the coils.

The RGA was calculated from

$$\text{RGA} = \text{SSGM} \bullet (\text{SSGM}^{-1})^T \tag{5}$$

and its elements evaluated by measuring the response of each control loop to a constant command signal u_i (4)

$$\text{RGA} = \begin{bmatrix} 1.1918 & -0.2031 & 0.0009 & 0.01 & 0 \\ -0.204 & 1.195 & 0.0002 & 0.0079 & 0.001 \\ 0.0035 & 0.0006 & 0.9957 & 0.0031 & 0.0017 \\ 0.0089 & 0.0075 & 0.0049 & 0.978 & 0.008 \\ -0.001 & 0.012 & -0.016 & 0.0006 & 0.99 \end{bmatrix}. \tag{6}$$

As suggested by Bristol, the pairing of variables for each control loop can be assigned from the position index of the RGA matrix elements. Positive elements nearest to 1 are the best choice [3]. These indexes define which input will control each output. Consequently, we adopt a $u_j - c_j$ pairing scheme, $j = 1 - 5$.

The RGA clearly shows that the last three pairs of variables are weakly coupled. Therefore, they can be considered as three independent SISO subsystems in a good approximation. On the contrary, the first two pairs are coupled, thus a 2×2 MIMO subsystem will be associated to the shimming function. A frequency response analysis of the RGA for this 2×2 MIMO subsystem

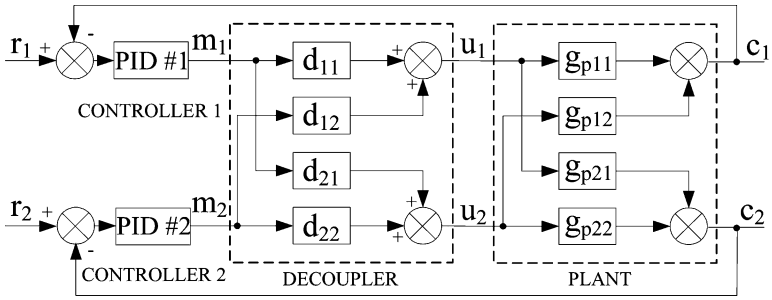

Fig. 5. Block diagram of the 2×2 MIMO control system and the decoupler. See text for details.

TABLE I
PARAMETERS OF THE CALCULATED TRANSFER FUNCTIONS

	$c_1=f(u_1)$	$c_2=f(u_2)$	$c_3=f(u_3)$	$c_4=f(u_4)$	$c_5=f(u_5)$
K_{ij}	13.347	10.2431	25.54	20.796	58.9
T_{ij}	520e-5	582e-5	510e-5	724e-5	410e-5
ω_{ij}	0.00136	0.0015	0.0014	0.0014	0.0014
ζ_{ij}	0.623	0.667	0.647	0.613	0.631

shows that their values remain constant over the entire bandwith of the compensating system.

From the SSGM we know the relative gain between inputs and outputs. However, to tune the system we still need to know the involved dynamics [9]. Based on the knowledge of the physics of the system, we proposed a second order transfer function with delay for each pair

$$g_{pij}(s) = \frac{K_{ij} e^{-sT_{ij}}}{\omega_{ij}^2 s^2 + 2\zeta_{ij}\omega_{ij} s + 1}. \tag{7}$$

In the last equation, $g_{pij}(s)$ is the transfer function in the Laplace domain (s) that relates the output i with the input j, K_{ij} is the gain as defined in the SSGM, T_{ij} is the delay time, ζ_{ij} is the damping factor, and ω_{ij} is the natural frequency.

For the SISO systems we may estimate the dynamics of the transfer functions $g_{p33}(s), g_{p44}(s)$ and $g_{p55}(s)$, while for the MIMO system it would be necessary to identify the dynamics of the transfer functions from each input to each output. As the dynamics of the magnetic field copies that of its driving current, the estimated dynamics for one output can be generalized to all other outputs generated by the same input (i.e., g_{p11} and g_{p21}). For the gradients, we will just identify the main diagonal of the transfer functions matrix (a matrix similar to the SSGM but including the complete transfer functions). The estimated parameters are listed in Table I. PIDs controllers were applied to each control circuit and individually tuned using different well known tuning methods. A decoupler was introduced between the controllers and the plant.

B. Decoupler

This block acts as a feedforward controller where a known disturbance (in this case the interaction between control circuits) is compensated before it affects the controlled variable. Fig. 5 shows the scheme of the 2×2 MIMO system. We define the associated transfer function matrix

$$G_p = \begin{bmatrix} g_{p11} & g_{p12} \\ g_{p21} & g_{p22} \end{bmatrix}. \tag{8}$$

where

- g_{pij} relates the c_i output with the u_j input;
- transfer functions of each row of the G_p matrix have the same dynamics (defined by the parameters of Table I);
- the gains of the transfer functions are defined by the SSGM matrix.

The aim of the decoupler D is that each input of the plant modifies only one output. That is

$$C = N \cdot M \Rightarrow \begin{bmatrix} c_1 \\ c_2 \\ \cdot \\ c_n \end{bmatrix} = \begin{bmatrix} n_1 & 0 & \cdot & 0 \\ 0 & n_2 & \cdot & 0 \\ \cdot & \cdot & \cdot & \cdot \\ 0 & \cdot & \cdot & n_n \end{bmatrix} \begin{bmatrix} m_1 \\ m_2 \\ \cdot \\ m_n \end{bmatrix}. \tag{9}$$

where $m_1, m_2, \ldots, m_n$ are the outputs of the PID controllers and $n_1, n_2, \ldots, n_n$ are the desired transfer functions for each control circuit for the decoupled plant.

The decoupled plant N (containing the decoupler D) has the same dimension that the original plant

$$N = G_p \cdot D. \tag{10}$$

Multiplying both sides of the last equation by G_p^{-1} we obtain D

$$D = G_p^{-1} N = \begin{bmatrix} d_{11} & d_{12} \\ d_{21} & d_{22} \end{bmatrix}. \tag{11}$$

The system has $n^2 + n$ unknown parameters and only n^2 equations. Thus, n degrees of freedom must be preset. We use as design parameters the desired open-loop transfer functions for each pair of controlled-manipulated variables (N). If we choose for the diagonal of N the same transfer functions appearing in the diagonal of G_p, each independently tuned PID controller will be applied to each closed loop. That is

$$N = \begin{bmatrix} g_{p11} & 0 \\ 0 & g_{p22} \end{bmatrix}. \tag{12}$$

Then, the decoupler transfer functions can be obtained from (11).

For a practical implementation of the transfer functions of the decoupler, it turns convenient to have equal denominators for

TABLE II
PID PARAMETERS

	PID of c_1	PID of c_2	PID of c_3	PID of c_4	PID of c_5
Sung method					
K_{Ci}	25e-3	23.4e-3	13.6e-3	13.5e-3	14.3e-3
T_{Ii}	2.69e-3	2.69e-3	2.68e-3	2.98e-3	2.70e-3
T_{Di}	1.57e-3	1.57e-3	1.54e-3	1.72e-3	1.57e-3
Morari IMC method (t_c= 0.1 τ)					
K_{Ci}	21.4e-3	20.7e-3	12.6e-3	10.4e-3	6.65e-3
T_{Ii}	1.69e-3	1.50e-3	1.81e-3	1.72e-3	1.77e-3
T_{Di}	4.23e-4	3.75e-4	4.53e-4	4.29e-4	4.42e-4
Morari IMC method (t_c= τ)					
K_{Ci}	11.8e-3	11.4e-3	6.95e-3	5.67e-3	3.66e-3
Morari IMC method (t_c=10 τ)					
K_{Ci}	2.14e-3	2.07e-3	1.26e-3	1.04e-3	6.65e-4
T_{Ii} and T_{Di} have the same values for all the PIDs calculed with the method of Morari.					

each row of G_p. On the contrary, the elements of the decoupler will not be causal [10]. After replacing the parameters of g_{pij} of Table I in the solution of (10), we get

$$d_{11} = 1.2352. \tag{13}$$

$$d_{12} = 0.43\frac{e^{-0.62e-3s}(1.85e-6s^2+1.69e-3s+1)}{(2.25e-6s^2+2e-3s+1)}. \tag{14}$$

$$d_{21} = 0.675\frac{e^{0.62e-3s}(2.25e-6s^2+2e-3s+1)}{(1.85e-6s^2+1.69e-3s+1)}. \tag{15}$$

$$d_{22} = 1.3. \tag{16}$$

The exponential term of (15) is positive. This transfer function is not causal and we must add a delay term $e^{-0.62e-3s}$ to all the elements of the decoupler. In this way we add an extra delay to the system that did not exist before, thus being a drawback of this control strategy. However, the addition of this delay improves the general performance of the system, as clearly seen in the simulations (Section IV-A).

C. Tuning of PID Controllers

All PID controllers were digitally implemented within PC environment in parallel configuration [13]

$$m_i(s) = K_{Ci}\left(1+\frac{1}{T_{Ii}}+\frac{T_{Di}s}{1+\frac{T_{Di}s}{P}}\right)[r_i(s)+c_i(s)], \tag{17}$$

where $i = 1,\ldots,5$; $m_i(s)$ is the i-controller output; $r_i(s)$ is the reference signal for the circuit of c_i (s); K_{Ci}, T_{Ii}, T_{Di} are the parameters of the i-controller; and P sets a pole to limit the derivative effect at high frequency

The value of P is usually chosen between 3 and 20. In the present case it was set to 10. To compare, we tuned the PIDs using the Sung's method [12] and the internal model control (IMC) design method [8]. The second method, has a tuning parameter t_c which is used to favor the output performance (small t_c) or the robustness (large t_c). We used three different values of t_c : $0.1\tau, \tau$ and 10τ, being τ the time delay which include the delay of the plant and the delay added by the decoupler (in the case of the gradients), resulting in a value of $\tau = T_{ij} + a_1$. The PID parameters obtained in each case are shown in Table II.

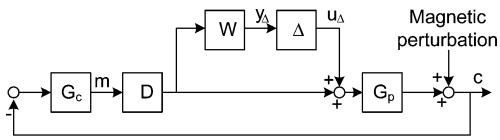

Fig. 6. Multiplicative input uncertainty affecting the system.

D. Stability and Robustness Analysis

Nominal Stability: Niederlinski theorem was used to verify the stability of the selected controlled-manipulated variables pairs [4]. Considering n individually stable control loops, the system with all their loops closed together will be unstable if and only if

$$\eta = \frac{|\mathrm{SSGM}|}{\prod_{i=1}^{n} K_{ii}} < 0. \tag{18}$$

Since we have $\eta = 4.7317$ the system is stable. This theorem gives necessary and sufficient stability conditions only for a 2×2 system. The system is stable independently whether the decoupler is used or not. This is a consequence from the fact that each loop was tuned using methods which ensures the individual stability *per se*. Nevertheless, as it will be seen later, the addition of a decoupler improves the performance.

Robust Stability: Each tuning method yields to different performance and particular robustness properties. We focus the robustness analysis on the process multiplicative input uncertainties because in this way, we can lump together sources of uncertainties like high frequency neglected dynamics and sensor gain model mismatch. In this way, we can compare the robustness of the system for the different tuning methods used in this work. Given a complex input multiplicative uncertainty (expressed as the product of a diagonal normalized complex matrix Δ and a weight matrix W), to study the robust stability of the system we express it in the general control configuration way (see Fig. 6) [6]. Within this picture, the PID controllers are represented by G_c

$$G_c = \begin{bmatrix} m_1 & 0 \\ 0 & m_2 \end{bmatrix}. \tag{19}$$

Then we consider the $M\Delta$-structure, that is, the transfer function associated to the perturbation (output u_Δ-input y_Δ). Considering a normalized model uncertainty, the system is robustly stable if

$$\det(I - M\Delta(s)) \neq 0, \quad \forall\omega, \forall\Delta \tag{20}$$

$$\Leftrightarrow \lambda_i(M\Delta) \neq 1, \quad \forall i, \forall\omega, \forall\Delta. \tag{21}$$

When the uncertainties are complex (unstructured uncertainty), we should consider the spectral radius function (ρ) which must satisfy

$$\rho(M\Delta(j\omega)) < 1, \quad \forall\Delta, \forall\omega. \tag{22}$$

The spectral radius of a matrix A is defined as their maximum autovalue

$$\rho(A) = \max_i |\lambda_i(A)|. \tag{23}$$

If Δ is allowed to be any complex transfer function matrix satisfying $\|\Delta\|_\infty < 1$, then the $M\Delta$-structure is robustly stable if and only if the maximum singular values $\bar{\sigma}(\cdot)$ of $M(j\omega)$ are

$$\bar{\sigma}(M(j\omega)) < 1 \quad \forall\omega. \tag{24}$$

It is also possible to define the structured singular value (μ) which provides of a generalization of the singular values and the spectral radius. To calculate μ, we must find first the smallest structured Δ which makes the matrix $I - M\Delta$ singular: $\mu(M) = 1/\bar{\sigma}(\Delta)$. That is

$$\mu(M) := \left\{ \min_{\Delta} [\bar{\sigma}(\Delta) \mid \det(I - M\Delta) = 0] \right\}^{-1}_{\text{for structured } \Delta}. \tag{25}$$

where

$$M = W G_{cd} G_p (I + G_{cd} G_p)^{-1} \tag{26}$$

$$G_{cd} = D\, G_c. \tag{27}$$

Then, the necessary and enough condition for robust stability for diagonal perturbations is

$$\mu(M(j\omega)) < 1, \quad \forall\omega. \tag{28}$$

When transfer functions matrices are converted to their space state representation, delays are included using the Pade approximation (we use order 6 to get a reasonable approximation of the time domain delay in compatibility with stability requirements). This approximation adds an inverse response due to the zeros that it introduces in the right half plane, thus weakening the whole system stability. However, if the approximated system turns stable, the stability of the real system is guaranteed.

We propose a diagonal unitary weight matrix W within the whole frequency range, and then we calculate the μ-function for our system using the D-K iteration algorithm [11] (see Fig. 7). Depending on how far is the value of μ at each frequency from 1, we know how far is the system from the instability limit (if $\mu < 1$), or how much must the uncertainty be reduced to became the system stable (if $\mu > 1$). We can observe that the PID tuned with the Morari method is more robust when we select a bigger value of t_c. The PID tuned with the Sung method has better robustness properties when a value of t_c equal to the delay of the plant is used.

IV. Experimental

Simulations were done using the Simulink tool of Matlab. The real system was digitally implemented at 2 KHz of sample frequency, with an anti aliasing filter fixed at 400 Hz.

A. Simulations

In Fig. 8 we can compare the B_x system output performance for different PID tuning parameters sets when a reference step signal is applied. We observe that the PID tuned with the Morari method shows a relevant overshoot at fast response. On the opposite, a small overshoot results for a slower system, compared with the system behavior when the PIDs are tuned with the Sung method. Considering the robustness analysis of Section III-D and the system output response, we conclude that controllers tuned with the Sung's method show a better compromise between robustness and output performance. Therefore, all following simulations and the real plant will be implemented using this tuning algorithm.

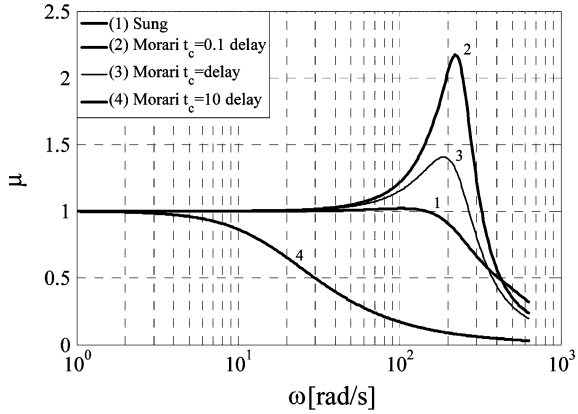

Fig. 7. μ-function for the different PID tuning parameters sets.

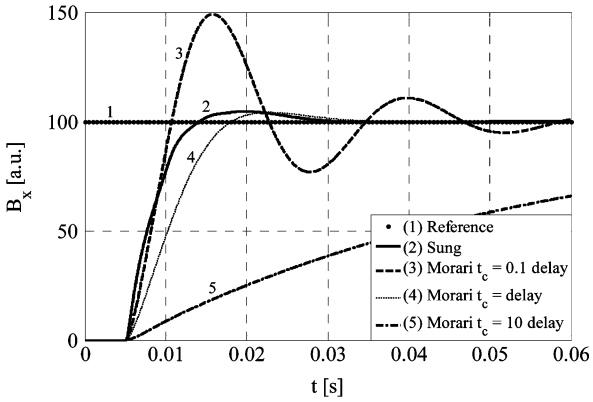

Fig. 8. Bx system response for different PID tuning parameters sets.

When a step is introduced in the reference signal r_1 of the G_{xx} loop, not only the value of G_{xx} becomes modified, but also both G_{yy} and G_{zz} (due to the interaction between variables). This phenomenon is the responsible for the dynamics performance degradation of the system when all loops are closed and no decoupler is used. The best results are obtained when the decoupler is used and the extra delay that it adds it is taken into account to tune the PIDs (Fig. 9).

Fig. 10 shows the behavior of the system against a step perturbation in G_{xx} of amplitude 300 [a.u.] introduced at $t = 5$ ms. We show here the rejection performance only for the more influenced variables, i.e., the gradients. It is important to note that due to the magnetic Gauss's law, the perturbation cannot be introduced only in G_{xx}. Damping occurs in about 10 ms.

B. Experimental setup and Measurements

Fig. 11 shows a block diagram of the hardware. The magnetic field was measured with the aid of ten A1321 Allegro

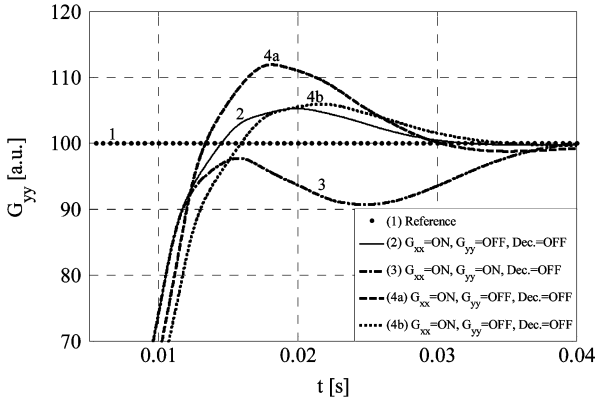

Fig. 9. Step response of G_{xx}: (1) Reference signal. (2) G_{xx} at closed loop ($\mathrm{G_{xx}} = \mathrm{ON}$) and G_{yy} at open-loop ($\mathrm{G_{yy}} = \mathrm{OFF}$), (3) G_{xx} and G_{yy} at closed loop without decoupler ($\mathrm{Dec.} = \mathrm{OFF}$) and (4a) G_{xx} and G_{yy} at closed loop with decoupler. (4b) Same as (4a), but with the PID tuned considering the delay added by the decoupler.

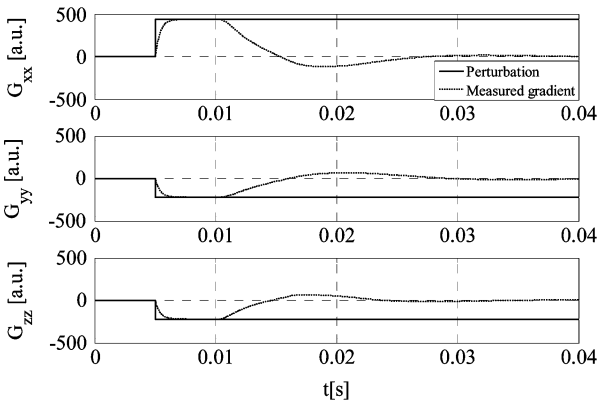

Fig. 10. Rejection response for a step-perturbation with the complete system (including decoupling) at closed-loop conditions.

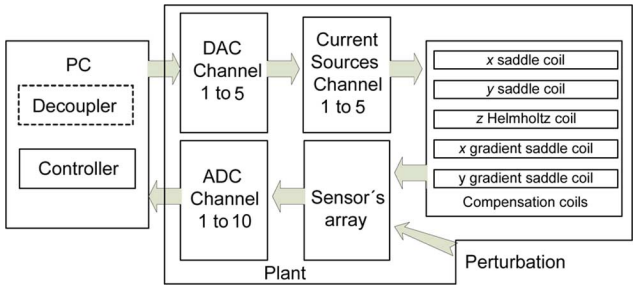

Fig. 11. Block diagram of the experimental setup.

Hall effect sensors. Their output signals were conditioned by means of instrumentation amplifiers designed using standard low cost TL082 operational amplifiers. Signals are read by the PC through a 14-bits resolution PCI726 Eagle data acquisition board. Control signals are applied to five current sources through five 8-bits AD0808 D/A converters. Finally, the five pairs of coils with their corresponding current sources generate the compensating magnetic field.

Performance Tests: As a first experiment, a change in the value of the command reference signal was applied to the x gradient loop. It can be seen in Fig. 12 that the influence of G_{xx} in G_{yy} is strongly dependent on whether the decoupler is used or not.

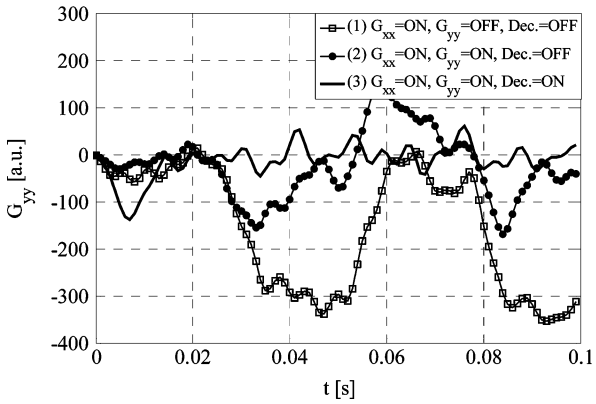

Fig. 12. Effect of the decoupler in the control system.

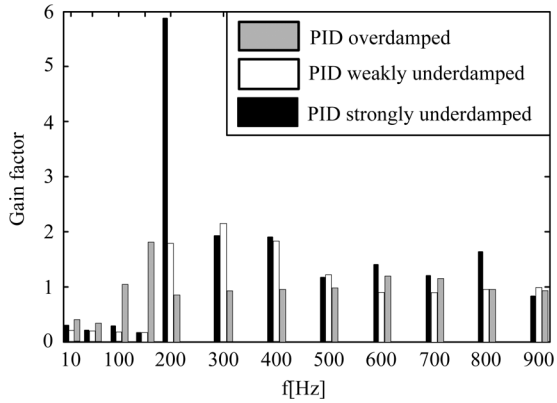

Fig. 13. Frequency response of the system (B_x channel) at different PID tuning conditions.

The system frequency response was analyzed by introducing a sine perturbation of constant magnitude at different frequencies. The gain factor was calculated for each frequency at three different tuning conditions of the PID regulators: a) using the PID as it was tuned with the Sung method (weakly underdamped), b) detuning PID of a) to make it overdamped and c) detuning PID of a) to make it strongly underdamped. As it can be seen in Fig. 13, for each tuning condition, the system attenuates the perturbation up to a critical frequency where it becomes amplified up to the limit fixed by the anti aliasing low pass filter. Higher frequencies will be rejected and they will not be affected by the active shielding (waterbed effect). For operation at the low-frequency end, the best performance was obtained with a weakly underdamped tuning.

Robustness Test: In Fig. 14 the system starts to cancel a gradient at $t = 0.5$ s when the plant is suddenly modified (model uncertainty) at $t = 1.25$ s. The system remains stable when the model variation is below the limits imposed by Fig. 7 (50% of gain variation and an addition of a pole at $\omega = 100$ r/s). However, it turns unstable for a gain variation of 300% and the addition of the same pole.

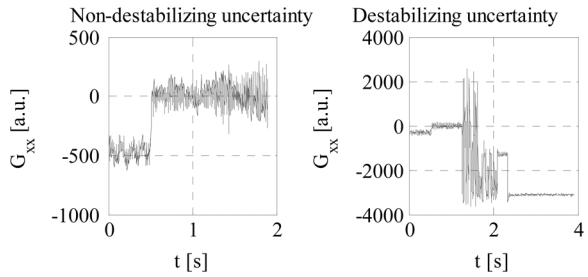

Fig. 14. Model uncertainty robustness test. The plant was modified at $t = 1.25$ s.

V. Conclusion

An elemental SHISHI compensating system was described. The presented approach, while limited to a very first approximation of the problem as required to its practical implementation, has the attractiveness of facilitating the test of different control strategies in a very simple way.

For both shimming and shielding an attenuation better than about 75% for external magnetic field components was obtained within a bandwidth of 150 Hz. Due to the coupling of the gradients a 2×2 MIMO subsystem was treated with a decoupler. Variable controllers were tuned independently with conventional methods as if they were all uncoupled SISO systems. The subject is still under active study.

Acknowledgment

The authors would like to thank Prof. M. Modesti for facilitating part of the hardware used at the beginning of the experimental setup.

References

[1] E. Anoardo and G. Ferrante, "Magnetic field compensation for field-cycling NMR relaxometry in the ULF band," *Appl. Magn. Reson.*, vol. 24, pp. 85–96, 2003.

[2] F. Bonetto, E. Anoardo, and M. Polello, "Saddle coils for uniform static magnetic field generation in NMR experiments," *Concepts Magn. Reson. Part B (Magn. Reson. Eng.)*, vol. 29B, pp. 9–19, 2006.

[3] E. H. Bristol, "On a new measure of interaction for multivariable process control," *IEEE. Trans. Autom. Contr.*, vol. 11, no. 1, pp. 133–134, Jan. 1966.

[4] J.-P. Corriou, *Process Control: Theory and Applications*. London, U.K.: Springer, 2004.

[5] C. Dedman, R. Dall, L. Byron, and A. Truscott, "Active cancellation of stray magnetic fields in a Bose-Einstein condensation experiment," *Rev. Sci. Instrum.*, vol. 78, p. 024703, 2007.

[6] J. C. Doyle, "Synthesis of robust controllers and filters," in *Proc. IEEE Con. Decision Control*, 1983, pp. 109–114.

[7] B. Hilgenfeld, E. Strahmel, H. Nowak, and J. Haueisen, "Active magnetic shielding for biomagnetic measurement using spatial gradient fields," *Physiol. Meas.*, vol. 24, pp. 661–669, 2003.

[8] M. Morari and E. Zafiriou, *Robust Process Control*. Englewood Cliffs, NJ: Prentice Hall, 1989.

[9] K. Ogata, *Modern Control Engineering*, 3rd ed. Englewood Cliffs, NJ: Prentice Hall, 1997.

[10] A. V. Oppenheim, A. S. Willsky, and I. T. Young, *Signals and Systems*. Englewood Cliffs, NJ: Prentice Hall, 1983.

[11] S. Skogestad and I. Postlethwaite, "Multivariable feedback control," in *Analysis and Design*. London, U.K.: Wiley, 2005.

[12] S. W. Sung, I. B. Lee, and J. Lee, "New process identification method for automatic design of PID controllers," *Automatica*, vol. 24, pp. 513–520, 1998.

[13] J. G. Ziegler and N. B. Nichols, "Optimum settings for automation controllers," *Trans. ASME*, vol. 64, pp. 759–768, 1942.